JOURNAL OF SYNCHROTRON RADIATION
ISSN 1600-5775

Muffin-tin potentials in EXAFS analysis

B. Ravel*

National Institute of Standards and Technology, Gaithersburg, MD 20899, USA.
*Correspondence e-mail: bravel@bnl.gov

Received 24 April 2015
Accepted 14 July 2015

Edited by S. M. Heald, Argonne National Laboratory, USA

Keywords: EXAFS; real-space multiple scattering; data analysis; muffin-tin potential.

Supporting information: this article has supporting information at journals.iucr.org/s

Muffin-tin potentials are the standard tool for calculating the potential surface of a cluster of atoms for use in the analysis of extended X-ray absorption fine-structure (EXAFS) data. The set of Cartesian coordinates used to define the positions of atoms in the cluster and to calculate the muffin-tin potentials is commonly also used to enumerate the scattering paths used in the EXAFS data analysis. In this paper, it is shown that these muffin-tin potentials are sufficiently robust to be used to examine quantitatively contributions to the EXAFS data from scattering geometries not represented in the original cluster.

1. Overview of muffin-tin potentials

In the decade from the mid-1980s to the mid-1990s, the main components of an analytical theory of extended X-ray absorption fine structure (EXAFS) were finalized and put into the form of user-oriented software. Three efforts from that era gained wide user bases and remain in use today (Gurman *et al.*, 1986; Filipponi *et al.*, 1995; Zabinsky *et al.*, 1995). These three efforts have much in common, each breaking the problem into three components, (1) calculation of the potential surface of a cluster of atoms, (2) enumeration of single scattering (SS) and multiple scattering (MS) configurations in the cluster and (3) calculation of the complex scattering function for configuration.

While this manuscript makes specific reference to *FEFF* (Zabinsky *et al.*, 1995), all three of the programs, in fact, use the same basic scheme for the calculation of the potential surface of the cluster, the *muffin-tin potential* model. In the muffin-tin (MT) model (Slater, 1937), neutral atoms (Ankudinov *et al.*, 1996) are placed at positions indicated by a list of Cartesian coordinates. This cluster is typically a few tens or hundreds of atoms and has no requirement of symmetry or periodicity. Each atom in the cluster, then, is defined by its three Cartesian coordinates and the Z number of its atomic species.

For most real materials, the coordinates of the atoms in the cluster result in interatomic distances that are shorter than the radii of the neutral atoms. Overlap of atoms is handled using some variation of the Mattheiss prescription (Mattheiss, 1964), in which Wigner–Seitz cells are created about each position in the cluster, then spheres are inscribed in the cells. These MT spheres are, in most cases, smaller than the neutral atom spheres, as shown schematically in Fig. 1. The MT spheres necessarily contain less electron charge than the larger neutral atom spheres. This excess charge is placed uniformly throughout the volume occupied by the cluster.

From these slightly charged spheres, the complex photoelectron scattering functions are computed using the default models in *FEFF* for the atomic potentials and the energy-

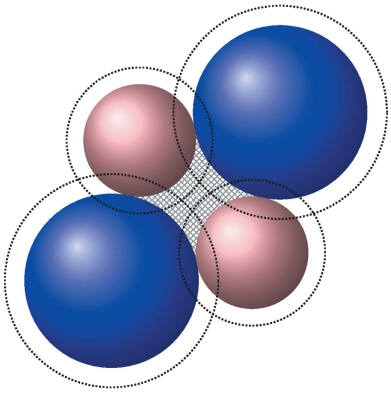

© 2015 International Union of Crystallography

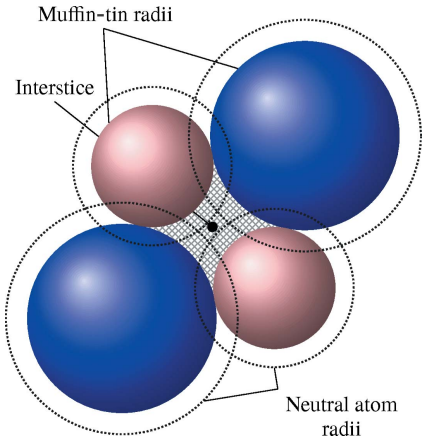

Figure 1
Schematic of the construction of the muffin-tin potential.

dependent Hedin–Lundqvist (Zabinsky *et al.*, 1995) self-energy. A majority of the EXAFS analysis in the literature has used this same potential model.

It is, perhaps, surprising that this model is so successful. This simple construction contains little chemistry. There is no mechanism to move charge between spheres, as expected of ionic bonding. Nor is there any concept of a covalent bond, which would imply excess charge density in certain directions. While both of those shortcomings can be improved upon in the theory, EXAFS analysis is regularly made without either improvement while still producing useful, defensible results. This is because the analysis of the EXAFS data typically begins about 3 Å^{-1}, or about 35 eV, above the absorption edge. In the EXAFS region, the photoelectron has high kinetic energy, thus is rather insensitive to the details of the potential surface.

2. Using muffin-tin potentials

Once the MT potentials are calculated and the paths are enumerated (Rehr *et al.*, 1992), the signal for each scattering contribution is computed for use in the EXAFS equation,

$$\chi_\Gamma(k) = \frac{NS_0^2 F_\Gamma(k)\exp(-2k^2\sigma_\Gamma^2)\exp[-2R_\Gamma/\lambda(k)]}{2kR_\Gamma^2} \times \sin\left[2kR_\Gamma + \delta_\Gamma(k)\right]. \quad (1)$$

Here, Γ is an index counting over all scattering paths considered in the fit. $F_\Gamma(k)$ and $\delta_\Gamma(k)$ are the amplitude and phase of the photoelectron scattering function as computed for scattering paths of any order using the MT potentials and the details of the individual scattering geometries.

The remaining terms – N, the path degeneracy; S_0^2, the passive electron reduction factor (Li *et al.*, 1995); R, the scattering path length; and σ^2, the mean square variation in scattering path length – are all parameterized using the variables of the fit. Additionally, an energy shift parameter, E_0, is used to align the zero of photoelectron wavenumber k in theory and data. Finally, $\lambda(k)$, the photoelectron mean free path, is also provided by the theory software. All paths used in the analysis are then summed,

$$\chi_{\rm theory}(k) = \sum_\Gamma \chi_\Gamma(k), \quad (2)$$

and compared with the measured $\chi(k)$.

In common practice, the list of Cartesian coordinates and Z numbers are used both for the calculation of the MT potentials and for the enumeration (Zabinsky *et al.*, 1995) of scattering contributions. In fact, MT construction and path enumeration are two separate chores that need not use the same input data. In this manuscript, a real data analysis problem is presented as an example of a situation where treating these two chores separately is fruitful.

3. Experimental methods

Polycrystalline $LaNiO_3$ was prepared by the citrate gel method described by Marcilly *et al.* (1970). Here, 0.01 mmol of $La(CH_3CO_2)_3{\cdot}H_2O$ and 0.01 mmol of $Ni(CH_3CO_2)_2{\cdot}4H_2O$ were dissolved in 20 ml of deionized water under stirring. To this solution was added 0.04 mmol of citric acid monohydrate dissolved in 5 ml deionized water, leading to the formation of a white precipitate. The pH was adjusted to circumneutral by dropwise addition of ammonium hydroxide (∼30% NH_3 basis) resulting in dissolution of the precipitate. The deep-green solution was evaporated at 343 K to form a rigid gel. The recovered gel was decomposed by heating at 523 K for 2.5 h in air to yield an amorphous precursor. X-ray powder diffraction demonstrated formation of single phase $LaNiO_3$ (black) after heating the amorphous precursors at 1173 K for 36 h under flowing oxygen. The mean particle size of the $LaNiO_3$ powder was estimated as 0.5 µm by scanning electron microscopy. The phase purity of the $LaNiO_3$ powder was verified by X-ray powder diffraction. See the supporting information for details about the preparation of the NiO sample.

A sample of $LaNiO_3$ was prepared for X-ray absorption spectroscopy (XAS) measurements by dispersing enough fine powder in polyethylene glycol to make an appropriate sample for the transmission XAS measurement. A pellet was then formed in a hydraulic press.

XAS data at the Ni K-edge (8333 eV) were measured at beamline X23A2 at the National Synchrotron Light Source at Brookhaven National Laboratory in New York, USA. This is an unfocused bend-magnet beamline using a Si(311) monochromator of a fixed-exit Golovchenko–Cowan (Golovchenko *et al.*, 1981) design. Harmonic rejection was made by a single bounce, flat, Rh-coated mirror. A nitrogen-filled ionization chamber was used to measure the incident and transmitted intensities as well as the intensity passing through a Ni foil used as a reference for energy alignment. There were $\sim 10^9$ photons s^{-1} in a spot of 5 mm in the horizontal and 0.5 mm in the vertical directions. At this low flux density, radiation-induced changes in speciation are not observed.

4. Analysis of $LaNiO_3$ data

To begin, the $LaNiO_3$ data were analyzed starting with its known crystal structures. $LaNiO_3$ crystallizes in a rhombohe-

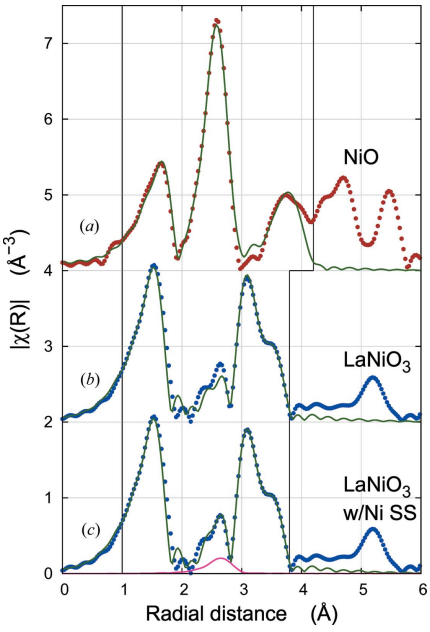

Figure 2
(*a*) Fit to a NiO (brown dots) standard using a simple fitting model based on its cubic halite structure. (*b*) Fit to $LaNiO_3$ (blue dots) using the known rhombohedral structure and the simple model described in the text. (*c*) Fit to the $LaNiO_3$ with the addition of a Ni SS path (pink) as described in the text. The solid green lines are the best fits in each case. The vertical lines represent the ranges over which the fits were evaluated.

dral modification of the perovskite structure (García-Muñoz *et al.*, 1992). This small rhombohedral distortion results in a splitting of the second shell La scatterers into a group of two La atoms at 3.29 Å and a group of six at 3.34 Å, while the first and third shells are unsplit with six O atoms at 1.93 Å and six Ni atoms at 3.84 Å. The variables of the fit included parameters for S_0^2 and E_0 as well as σ^2 for the O, La and Ni single-scattering paths. Because the distortion away from the cubic perovskite structure is small, the approximation of a fitted isotropic expansion coefficient α is used in each path to compute the change in R as $\Delta R = \alpha R_0$, where R_0 is the path length in the *FEFF* calculation. Various MS paths are included in the fit and parameterized without introducing any new fitting variables. Analysis was performed using the *ARTEMIS* program (Ravel & Newville, 2005; Newville, 2001). This simple model yields a reasonably good fit as seen in Fig. 2(*b*). All parameters yield reasonable values, as seen in the left-hand column of Table 1. Still, there is significant misfit in the region from 2.2 Å to 2.8 Å, a region dominated in the $LaNiO_3$ structure by single scattering from the La atoms.

This sample, then, represents a common situation encountered in the course of EXAFS analysis. The fit is mostly reasonable, but there is something obviously missing. The point of this manuscript is to present a powerful, flexible tool for solving an analysis challenge like this.

5. Addition of a Ni SS path

The fit shown in Fig. 2(*b*) uses *all* of the paths in the $LaNiO_3$ structure with path lengths of 3.87 Å or less. There is nothing

Table 1
Results of the fits discussed in the text.

1σ uncertainties, calculated as the diagonal elements of the covariance matrix of the fit, are given in parentheses. Only the portion of the NiO fit immediately relevant to the $LaNiO_3$ analysis is shown, see the supporting information for more information about the NiO fit.

	$LaNiO_3$	With SS path	NiO
S_0^2	0.72 (5)	0.72 (4)	
E_0	−3.05 (57) eV	−3.18 (54) eV	
α	−0.002 (1)	−0.002 (1)	
$\sigma^2_{\rm O}$	0.00307 (81) Å^2	0.00305 (77) Å^2	
$\sigma^2_{\rm La}$	0.00569 (59) Å^2	0.00579 (59) Å^2	
$\sigma^2_{\rm Ni}$	0.00537 (80) Å^2	0.00538 (76) Å^2	
N:Ni		0.80 (45)	12
R:Ni		3.003 (105) Å	2.951 (4) Å
σ^2:Ni		$\equiv \sigma^2_{\rm Ni}$	0.00539 (56) Å^2

from the $LaNiO_3$ structure not included in the fit that can contribute the additional spectral weight in the region from 2.2 Å to 2.8 Å. The check for phase purity described in §3 was made by X-ray diffraction. Only the *diffracting* portion of the sample is necessarily pure $LaNiO_3$. There is a possibility that some Ni could be contained in a poorly diffracting oxide that may be nanoscale or amorphous. The NiO data shown in Fig. 2(*a*) supports this assumption – the large contribution from the second shell Ni scatterer in NiO is at just the right location to account for the missing spectral weight in the 2.2 Å to 2.8 Å region.

As part of the potentials calculation for $LaNiO_3$, an MT potential for Ni was calculated. However, there are no Ni scatterers in the 2.2 Å to 2.8 Å range in the $LaNiO_3$ structure. In *FEFF*, the part of the program that performs path enumeration writes a file called `paths.dat`. This is a plain text file that, for each scattering path, has a paragraph which gives the Cartesian coordinates of the atoms in that path. This file, along with the information about the potentials, is used by the part of the program that generates the complex scattering functions for use in the EXAFS equation.

To investigate the prospect of a Ni scatterer, a `paths.dat` file is created with a single paragraph describing a SS path with the Ni absorber and a Ni scatterer at the position (0, 0, 2.97). *FEFF* uses the Ni MT potential from the $LaNiO_3$ calculation and this specially crafted `paths.dat` file to generate the Ni SS contribution to the EXAFS at that distance.

The result of a fit using this specially crafted SS path is shown in Fig. 2(*c*) with the contribution from that path shown in pink. The addition of this SS path resolves most of the misfit in the 2.2 Å to 2.8 Å region. This path was parameterized with its own fitting variables, see the third column of Table 1, for N, ΔR and σ^2. The S_0^2 and E_0 from the $LaNiO_3$ portion of the fitting model were used for this path. The parameters related to $LaNiO_3$ change only slightly with the addition of the Ni SS path.

Comparing the result for N with the 12 Ni neighbors in bulk NiO, we can approximate the fraction of Ni atoms in the poorly diffracting oxide phase as 6.3 (3.5)%. The R value is consistent within error bars with the value from the analysis of NiO. When the σ^2 parameter for the Ni SS path was floated

freely, the fit proved unstable, yielding ill-defined values for all three parameters. This is likely because of the small contribution of the Ni SS path to the entire EXAFS spectrum. Noting that the σ^2 for the Ni second neighbor in NiO is very close to the σ^2 for the Ni scatterer in $LaNiO_3$, the σ^2 for the Ni SS path was constrained to that value. This stabilized the fit, resulting in the N and R values reported in Table 1.

While adding the Ni SS path certainly does make the fitted spectrum look more like the data, the fit in Fig. 2(*c*) is defensible not because it is closer to the data than in Fig. 2(*b*) but for reasons of chemistry and statistics. The assumption that an amorphous metal oxide might precipitate during sample preparation is both reasonable and common when using sol–gel synthesis. Further, as discussed in the supporting information, the addition of the N and R fitting parameters improved the quality of fit, as seen by a reduction in the χ^2_ν fitting metric. This result is chemically and statistically defensible and not merely an *ad hoc* alteration of a fitting model.

6. Discussion

To understand why this method of constructing a SS path works so well in the analysis, consider the nature of the MT potential. The main parameters of the potential are the atomic species of the scatterer and the size of the MT sphere. In the NiO *FEFF* calculation, the MT radius of the Ni^{2+} ion is 1.154 Å, for the Ni^{3+} in the $LaNiO_3$ *FEFF* calculation it is 1.034 Å. In fact, any real crystal containing Ni and O will have a nearest neighbor around 2 Å, resulting in a similar value for the Ni MT radius.

In Fig. 3, the contribution from a single Ni atom in the second shell of NiO (blue) is compared with the contribution from the Ni SS path computed using the MT potentials from the $LaNiO_3$ calculation (red). Despite the difference in MT radii, the computed $\chi(k)$ are nearly identical, with most of the difference in k being below the range of the Fourier transform. The substantial advantage of computing a scatterer at about the right distance out-weighs the small error introduced by the slightly incorrect MT radius. Fitting the $LaNiO_3$ data using the second shell of NiO in place of the Ni SS path results in a nearly identical fit. This is shown in detail in the supporting information.

In the *ARTEMIS* program, the implementation of the SS path requires the user to select a scatterer species from a *FEFF* calculation that has already been run and to specify a distance between the absorber and the scatterer.

One possible counterpoint to this presentation is that NiO is a well known, readily available standard. It is easy to run *FEFF* on the known NiO structure (Wyckoff, 1963) and to use the Ni SS path from that calculation in the fit to the $LaNiO_3$ data. While that would be a fine strategy in this case, there are several reasons the method presented here – reusing MT potentials from an existing calculation with specially crafted scattering geometries – is attractive.

Once implemented in a data analysis program, this way of making scattering contributions provides a quick, convenient

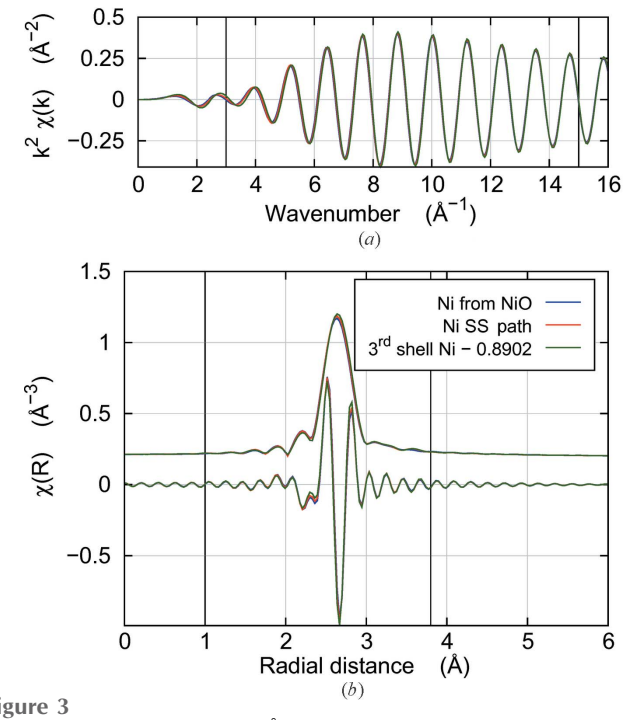

Figure 3
(*a*) A single Ni atom at 2.9475 Å, computed using the NiO MT potentials (blue) and the $LaNiO_3$ MT potentials (red), as $\chi(k)$. The third trace (green) shows the third shell Ni scatterer from $LaNiO_3$ shifted by 0.8902 Å to 2.9475 Å. (*b*) The magnitude and real part of the Fourier transforms of those three calculations. The vertical black lines represent the Fourier transform and fitting ranges used in the analysis of the data from the mixed sample.

way to test specific scatterers at specific distances against the data being analyzed. It allows for the investigation of absorber–scatterer pairs at distances that might be hard to find in a well characterized standard or an established crystal structure.

A second possible counterpoint is that a large ΔR can be applied to the Ni path at 3.838 Å in the $LaNiO_3$ structure to shift it to a position near 3 Å. This is shown as the green trace in Fig. 3. This is substantively similar to the calculation using the NiO MT potentials, but with larger (albeit still small) deviation below 5 $Å^{-1}$ resulting from the R dependence of the computation of the complex scattering function from the MT potentials. Whether the approach of applying a large ΔR is more or less complicated than the path construction suggested in this manuscript is an implementation detail of the data analysis software.

Extending this method to MS is a trivial extension of the procedure described in §5. Any MS path could be computed by providing either a set of Cartesian coordinates or a set of lengths and scattering angles. Consider a material for which nominally collinear MS paths can deviate from collinearity when lattice distortions are considered in a fitting model. Examples of this sort of analysis in the literature tend to use approximations to the effect of a small deviation from collinearity on these important MS paths. One such example is given by Frenkel *et al.* (1996). Constructing MS paths in this way would be a more accurate, low-overhead mechanism for

incorporating the effect of a variable scattering angle in the EXAFS fitting loop.

Acknowledgements

The author thanks J. Woicik of NIST for discussion of a very similar sample and M. Stennett and N. Hyatt of the University of Sheffield for providing the $LaNiO_3$ and NiO samples. Use of the National Synchrotron Light Source, Brookhaven National Laboratory, was supported by the US Department of Energy, Office of Science, Office of Basic Energy Sciences, under contract No. DE-AC02-98CH10886.

References

Ankudinov, A., Zabinsky, S. & Rehr, J. (1996). *Comput. Phys. Commun.* **98**, 359–364.
Filipponi, A., Di Cicco, A. & Natoli, C. R. (1995). *Phys. Rev. B*, **52**, 15122–15134.
Frenkel, A., Stern, E., Voronel, A. & Heald, S. (1996). *Solid State Commun.* **99**, 67–71.
García-Muñoz, J. L., Rodríguez-Carvajal, J., Lacorre, P. & Torrance, J. B. (1992). *Phys. Rev. B*, **46**, 4414–4425.
Golovchenko, J., Levesque, R. A. & Cowan, P. L. (1981). *Rev. Sci. Instrum.* **52**, 509–516.
Gurman, S., Binsted, N. & Ross, I. (1986). *J. Phys. C*, **19**, 1845–1861.
Li, G., Bridges, F. & Booth, C. (1995). *Phys. Rev. B*, **52**, 6332–6348.
Marcilly, C., Courty, P. & Delmon, B. (1970). *J. Am. Ceram. Soc.* **53**, 56–57.
Mattheiss, L. F. (1964). *Phys. Rev.* **133**, A1399–A1403.
Newville, M. (2001). *J. Synchrotron Rad.* **8**, 322–324.
Ravel, B. & Newville, M. (2005). *J. Synchrotron Rad.* **12**, 537–541.
Rehr, J. J., Albers, R. C. & Zabinsky, S. I. (1992). *Phys. Rev. Lett.* **69**, 3397–3400.
Slater, J. C. (1937). *Phys. Rev.* **51**, 846–851.
Wyckoff, R. (1963). *Crystal Structures.* New York: Wiley.
Zabinsky, S. I., Rehr, J. J., Ankudinov, A., Albers, R. C. & Eller, M. J. (1995). *Phys. Rev. B*, **52**, 2995–3009.

JOURNAL OF SYNCHROTRON RADIATION

Volume 22 (2015)

Supporting information for article:

Muffin-tin potentials in EXAFS analysis

B. Ravel

1 Supplemental materials: Muffin tin potentials in EXAFS analysis

1.1 XANES data for $LaNiO_3$ and NiO

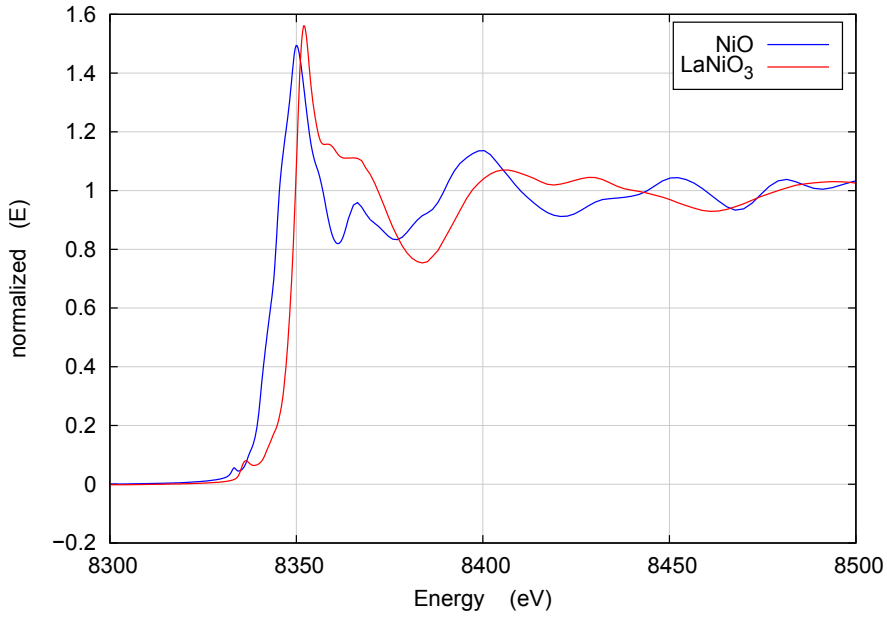

Figure 1: XANES data for NiO (blue) and $LaNiO_3$ (red).

1.2 $LaNiO_3$ phase purity

X-ray powder diffraction data were acquired in θ-2θ mode with a Bruker D2 Phaser[1], operating with Cu Kα radiation and a Lynxeye position sensitive detector (a Ni filter was used to remove Cu Kβ radiation). The angular range was $20° < 2\theta < 80°$, with a step size of 0.02° and a count time of 2 seconds per step.

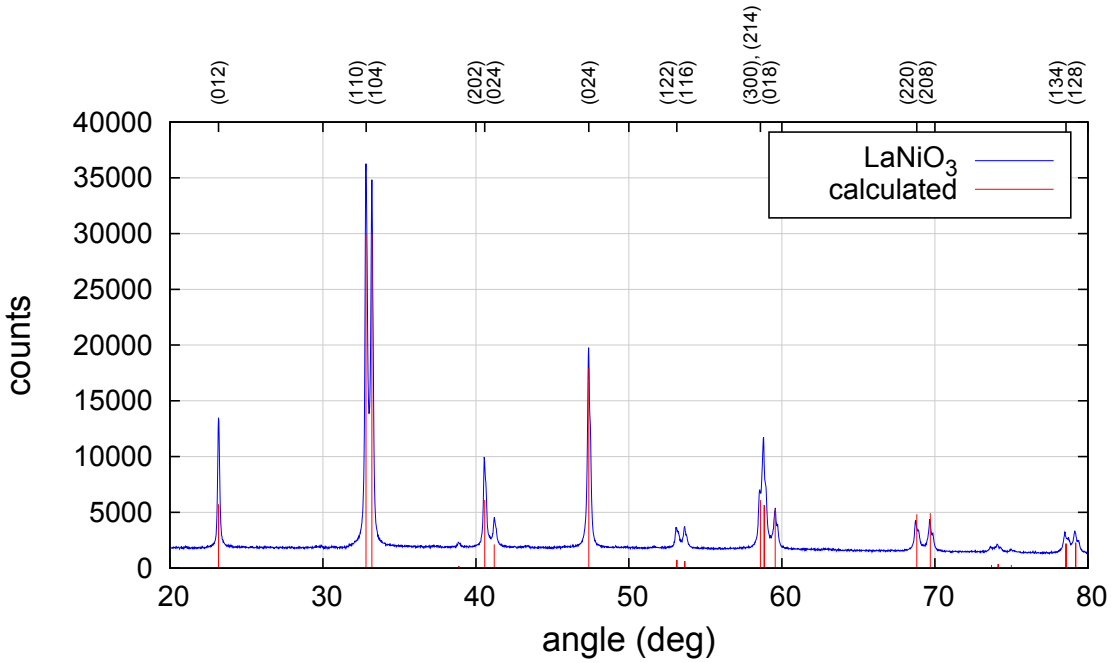

Figure 2: Diffractogram of the $LaNiO_3$ sample compared with peak positions and intensities computed from the known crystal structure.

[1]Any mention of commercial products is for information only; it does not imply recommendation or endorsement by NIST.

1.3 NiO sample preparation

Polycrystalline NiO was prepared by the same method as described in the main text for $LaNiO_3$. To achieve similar particle size, we started with 0.01 mmol of $Ni(CH_3CO_2)_2{\cdot}4H2O$ dissolved in 10 ml of deionised water with the addition of 0.02 mmol of citric acid monohydrate. X-ray powder diffraction demonstrated formation of single phase NiO (olive green) after heating the amorphous precursors at 900° C for 36 hours under flowing oxygen. The mean particle size of the NiO powder was estimated as 2.0 μm by scanning electron microscopy.

A sample of NiO was prepared for X-ray Absorption Spectroscopy (XAS) measurements by dispersing enough fine powder in polyethylene glycol to make an edge step around 0.5. A pellet was then formed in an hydraulic press.

1.4 Analysis of the NiO EXAFS data

NiO is halite structured and analyzed to a radial distance which includes the first four coordination shells. The variables in this fit included parameters for S_0^2, E_0, an isotropic lattice expansion coefficient α, and σ^2 parameters for each of the four single scattering paths. Various multiple scattering paths were included in the fit and parameterized without introducing new variables to the fit.

S_0^2	0.70(5)
E_0	−0.79(55)
α	0.0013(15)
σ^2 – O, 1^{st} shell	0.00476(126)
σ^2 – Ni, 2^{nd} shell	0.00539(56)
σ^2 – O, 3^{rd} shell	0.03217(2058)
σ^2 – Ni, 4^{th} shell	0.00713(95)

Table 1: Results of fit to NiO using the cubic halite model. The unit of E_0 is eV and of σ^2 is Å^2.

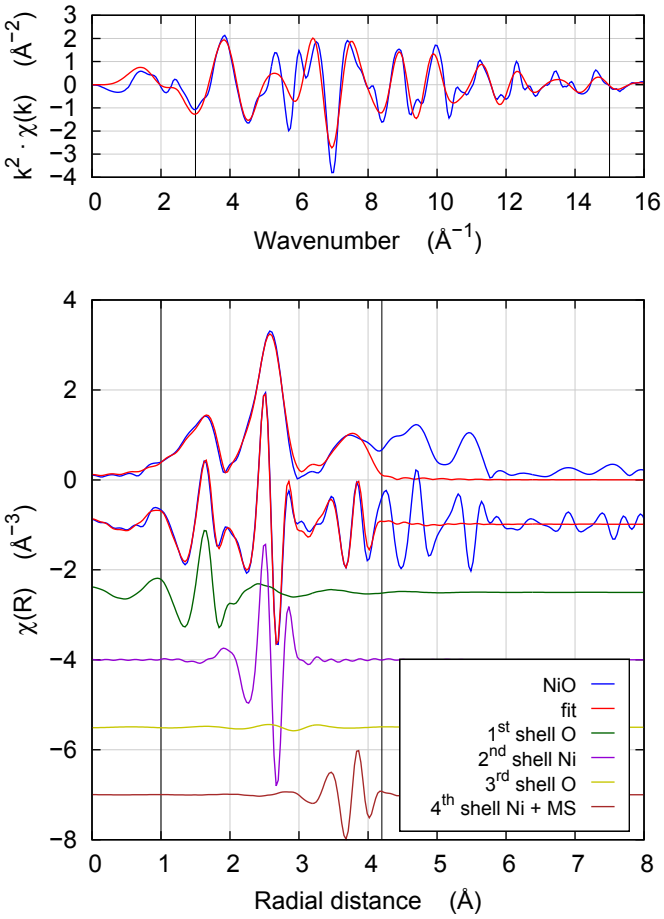

Figure 3: Fit to NiO using the cubic halite structure. The brown line includes the contribution from the fourth shell Ni scatterer plus several collinear MS paths at the same distance. The vertical lines show the ranges of the Fourier transform in k and the fit in R.

1.5 $LaNiO_3$ fit using the constructed Ni SS path

Upon addition of the Ni SS path (brown line in Fig. 4), the fit improved statistically. The R-factor reduced from 0.023 to 0.020. The inclusion of the Ni SS path added 2 floating parameters, taking the fit from 6 to 8 parameters and reducing the freedom ν of the fit from about 15 to about 13. The reduced chi-square χ^2_ν went from 576 to 533 upon addition of the Ni SS path. See Table 1 in the main text.

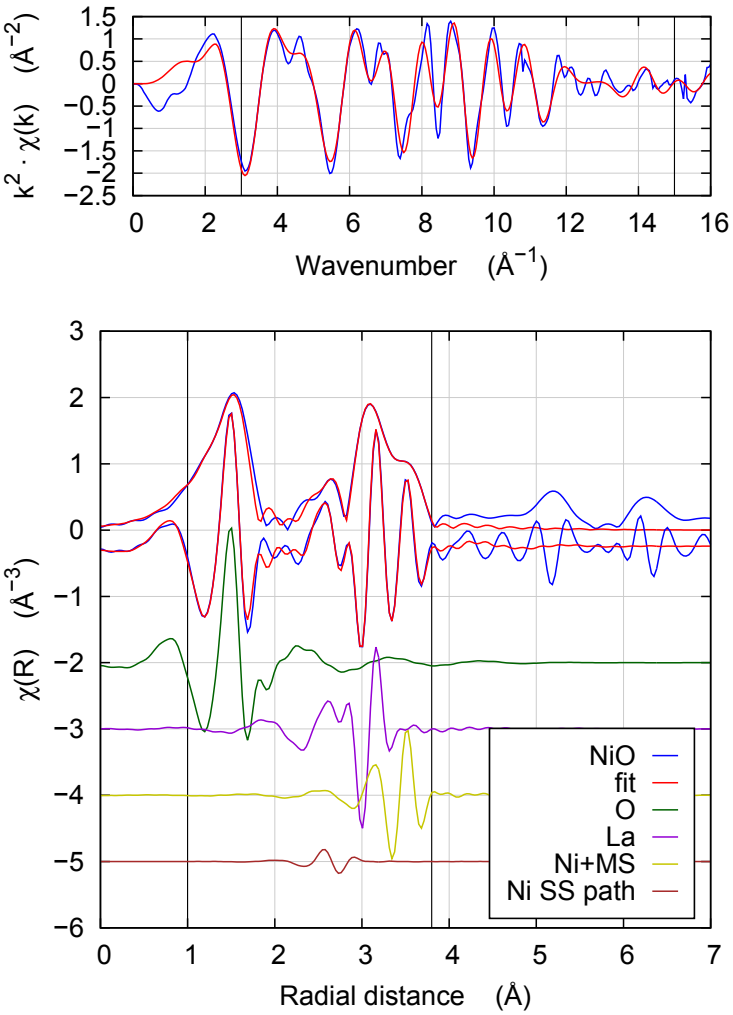

Figure 4: Fit to $LaNiO_3$ using the constructed Ni SS path. The yellow line includes contributions from the third shell Ni scatterer plus several multiple scattering paths at the same path length. The brown line is the Ni SS path added to represent the contribution from the non-diffracting Ni oxide. The vertical lines show the ranges of the Fourier transform in k and the fit in R.

1.6 $LaNiO_3$ fit using the Ni path from NiO

The figure below shows the same fit as in Sec. 1.5 of this supplemental document excpet that the Ni scatterer at about 3 Åis repesented in the fit by the 2^{nd} shell Ni scatterer from NiO. The R-factor here is 0.020 and the reduced chi-square χ^2_ν is 531, both equivalent to the fit with the Ni SS path shown in Sec. 1.5. The number of Ni atoms in the poorly-diffracting NiO phase determined from this fit is 6.8(4.0)% and their R is 3.000(35) Å, both consistent with the results given in the main text.

On visual inspection, this fitting result is indistinguishable from the result shown in Sec. 1.5 using the Ni SS path.

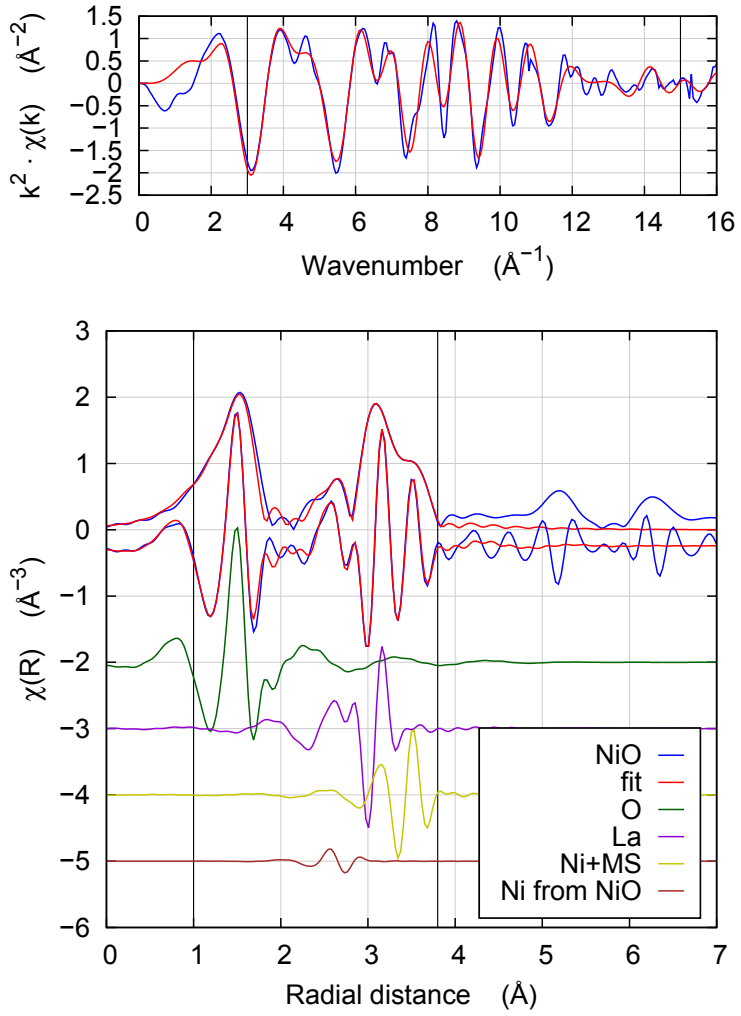

Figure 5: Fit to $LaNiO_3$ using the 2^{nd} shell Ni path from NiO. The yellow line includes contributions from the third shell Ni scatterer plus several multiple scattering paths at the same path length. The brown line is the 2^{nd} shell Ni path from NiO used to account for the non-diffracting Ni oxide. The vertical lines show the ranges of the Fourier transform in k and the fit in R.